Absolute radiant flux measurement of the angular distribution of synchrotron radiation

Ping-Shine Shaw, Uwe Arp, and Keith R. Lykke
National Institute of Standards and Technology, Gaithersburg, Maryland 20899, USA
(Received 17 March 2006; published 11 July 2006)

We have measured the absolute radiant flux of synchrotron radiation as a function of the angle above and below the orbital plane with high accuracy at the Synchrotron Ultraviolet Radiation Facility (SURF III) at the National Institute of Standards and Technology (NIST), and the results were compared with theoretical calculations. The radiant flux of synchrotron radiation was measured at effective wavelengths of 256.5, 397.8, and 799.8 nm using three calibrated narrow-band filter radiometers with electron energies ranging from 180 to 380 MeV at SURF III. The filter radiometers were positioned inside a beamline with an unobstructed view of synchrotron radiation. The measured radiant flux agrees with theoretical Schwinger formulation to better than 0.5% for angles up to several milliradians.

DOI: 10.1103/PhysRevSTAB.9.070701 PACS numbers: 41.60.Ap, 42.72.Bj, 07.60.Dq

I. INTRODUCTION

The mathematical formulation of synchrotron radiation emission based on the Maxwell equations for a relativistic charged particle was well established after Schwinger's work [1] more than half a century ago. The formulation, known now as the Schwinger's equation, is the foundation for the rapidly expanding number of synchrotron facilities and pivotal in the development of more recent generations of synchrotron radiation sources such as wigglers, undulators, and free-electron lasers [2].

In the early days of dedicated storage ring synchrotron light sources, there were considerable efforts [3–6] devoted to comparing the measured characteristics of synchrotron radiation with Schwinger's prediction. The reasons for such studies were twofold: first, to confirm Schwinger's analysis, and second, to provide a solid basis for the use of synchrotron radiation as an absolute and calculable radiometric source. The first measurements of the spectral and angular distributions by Elder *et al.* [3] and Tomboulian *et al.* [4] were in agreement with the Schwinger equation to the limited accuracy achieved at that time. Later, Codling *et al.* [5], measured the angular distribution of visible light from the 180 MeV Synchrotron Ultraviolet Radiation Facility (SURF I) at the National Bureau of Standards using a filter detector package and photographic films. They found agreement with theory in the relative shape of angular distribution but the measurement accuracy was limited by significant uncertainties in the machine parameters and detector calibration.

As synchrotron radiation sources became more sophisticated, comparison of Schwinger's equation with measurements was mostly left to researchers performing synchrotron-based radiometry [7–17] as a way to verify machine performance. Almost all of these studies involved comparing the spectral distribution of synchrotron radiation at a fixed viewing angle with other standard sources such as a blackbody source. Only a few reports on radiometry [14–17] described angular distribution measurements. Among them, some measurements were either relative or with high uncertainty [14,15]. Others were limited to one electron energy and a few wavelengths in the visible or near IR [16,17]. Furthermore, direct comparison of measurement results with the Schwinger equation evaluated at a fixed wavelength is complicated by the bandwidth of the detector. To the best of our knowledge, a comprehensive study relating accurate measurements at different angles and energies to the prediction of the Schwinger's equation has not been documented.

Part of the reason for the paucity of absolute radiant measurements of the angular distribution of synchrotron radiation arises from technical difficulties associated with most modern synchrotron radiation facilities. These facilities typically use high energy electrons (several GeV) to generate a high flux of x rays. However, absolute radiant flux measurements are best conducted in the UV-visible region because current detector technology enables the most accurate radiation flux measurements in this spectral region. High doses of x rays tend to degrade the performance of UV-visible detectors. In addition, to perform the absolute angular distribution of synchrotron radiation in the UV-visible requires a large acceptance angle (tens of mrad), access that is difficult to have in the long beamlines of the modern facilities. A low energy (several hundreds MeV) storage ring with the flexibility of operating at a range of electron energies is best suited for the absolute measurement of the angular distribution of synchrotron radiation. For high-accuracy radiation measurements, it is also imperative to have storage ring parameters accurately determined and to minimize the scattered light from the vacuum walls of the storage ring and the beamline.

One of the few synchrotron radiation facilities that fits this profile is the SURF III [18] machine at the National Institute of Standards and Technology (NIST). The SURF

III storage ring is a unique textbook case circular orbit with a radius of 83.8 cm and variable electron energies from 10 MeV up to 380 MeV. The magnetic field along the orbit can be accurately measured and the variation of the field throughout the circular orbit is less than 10^{-4}. Other machine parameters, orbital radius and electron beam current, that are used in Schwinger's equation are also determined with high accuracy.

In addition to the requirements on the synchrotron parameters, the detector used for measurements must be well calibrated with high accuracy. To acquire spectral information, the detector can be used either with a monochromator or a narrow-band filter. Generally, monochromators have better resolution than filters, but less accurate calibration in absolute irradiance response. For detectors with filters, the absolute spectral response must be mapped out so that variation in response due to the spectral shape of synchrotron radiation can be accounted for.

Here, we report the absolute radiant flux measurement of the angular distribution of synchrotron radiation at SURF III and comparison with Schwinger's equation. The goal is to compare measurements with theoretical calculations to the highest accuracy possible. With three filter radiometers, we effectively measured the angular distributions at three wavelengths from UV to near IR, 256.5, 397.8, and 799.8 nm, at several different electron energies from 105 to 380 MeV. We picked these wavelengths because NIST's detector calibration capability has the lowest uncertainties in this spectral range. Filter radiometers were constructed using silicon photodiodes coupled with a precision aperture and a narrow-band interference filter. Calibration of the spectral irradiance responsivities of these filter radiometers was performed with a scale derived from a high-accuracy cryogenic radiometer. Unlike previous angular distribution studies, a formulation is developed so that comparison of the filter radiometer measurement and Schwinger equation can be made at a single wavelength instead of having to integrate the Schwinger equation over the bandwidth of the filter radiometer. Also, the filter radiometers were irradiated directly with synchrotron radiation in vacuum without any interfering windows, thus eliminating the uncertainty caused by the transmission of the window.

In this paper, we start with a detailed analysis on the implication of measuring synchrotron radiation flux using a filter radiometer with a finite bandwidth. A simple numerical technique is proposed to derive absolute spectral irradiance at a fixed wavelength from the signal of the filter radiometer exposed to synchrotron radiation. In Sec. III, we discuss the experimental setup for the angular distribution measurement with filter radiometers, SURF III, and the beamline used for this study. In Sec. IV, the technique and the results of filter radiometer calibration is described. Finally, the results of the measured angular distributions are compared with theoretical calculation from the Schwinger equation in Sec. V.

II. RADIANT FLUX MEASUREMENT OF SYNCHROTRON RADIATION USING FILTER RADIOMETERS

The derivation of Schwinger's equation generally starts from the basic equation relating the far field of the electric field generated by a moving charge [19]

$$\mathbf{E}(\mathbf{x}, t) = \frac{e}{c}\left[\frac{\mathbf{n} \times \{(\mathbf{n} - \boldsymbol{\beta}) \times \dot{\boldsymbol{\beta}}\}}{(1 - \boldsymbol{\beta} \cdot \mathbf{n})^3 R}\right]_{\text{ret}}, \tag{1}$$

where R and $\mathbf{n}$ are the distance and unit vector from the charge to the observer at $\mathbf{x}$, respectively. $\boldsymbol{\beta}$ is the velocity vector of the charge normalized by the speed of light. The right-hand side of the electric field expression is evaluated at the retarded time $t' = t - R(t')/c$.

Given the electric field from Eq. (1), the spectral distribution of the resulting radiation is given by

$$\frac{d^2 I}{d\omega d\Omega} = \frac{c}{2\pi}\left|\sqrt{\frac{1}{2\pi}}\int_{-\infty}^{\infty} R\mathbf{E}(\mathbf{x}, t)e^{i\omega t}dt\right|^2. \tag{2}$$

Applying the above equations to a charge moving in a circular motion, one can derive Schwinger's equation which expresses the flux of synchrotron radiation emitted by a relativistic charge e into a solid angle $d\Omega$ at a wavelength of λ as [19]

$$\frac{d^2 I}{d\lambda d\Omega} = \frac{27e^2}{32\pi^3\rho^2}\left(\frac{\lambda_c}{\lambda}\right)^4 \gamma^8(1 + \gamma^2\psi^2)^2\left[K_{2/3}^2(z) + \frac{\gamma^2\psi^2}{1 + \gamma^2\psi^2}K_{1/3}^2(z)\right] \tag{3}$$

with

$$z = \frac{1}{2}\frac{\lambda_c}{\lambda}(1 + \gamma^2\psi^2)^{3/2}.$$

In the above equations, ρ is the radius of curvature of the electron's orbit, ψ is the observer's angle above or below the orbital plane, $K_{2/3}$ and $K_{1/3}$ are modified Bessel functions, λ_c is the critical wavelength defined as

$$\lambda_c = \frac{4\pi\rho}{3\gamma^3},$$

and

$$\gamma = \frac{E}{m_e c^2},$$

where E is the electron energy, m_e is the mass of the electron, and c is the speed of light. The two modified Bessel functions on the right-hand side of Eq. (3) represent the contribution from horizontal and vertical polarization, respectively. An example of the calculated SURF III angular distributions at 400 nm for electron energies of 380 and 105 MeV are shown in Fig. 1.

One should note that several approximations were made in the derivation of Schwinger's equation. In order to

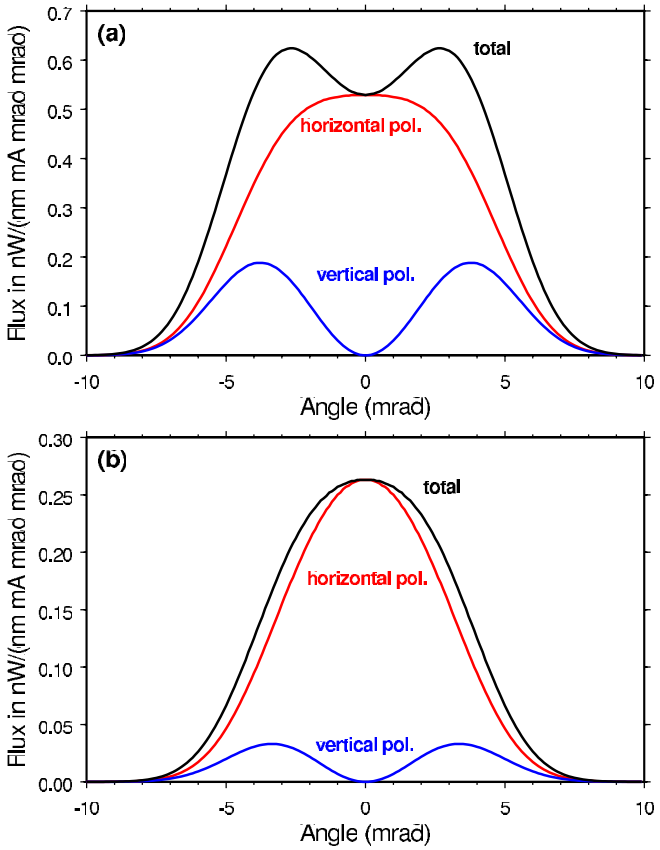

FIG. 1. (Color) Calculated angular distribution of synchrotron radiation in the vertical direction at 400 nm using SURF III parameters and 1 mA of current for (a) 380 MeV and (b) 105 MeV electron energy. The orbit is in the horizontal plane. The curves shown represent radiation from two different polarization states as well as their sum.

assess the accuracy of Schwinger's equation, we have developed computer codes to numerically calculate the flux of SURF III synchrotron radiation directly from Eqs. (1) and (2) without any approximation. We found that, for electron energies and wavelengths used in this work, the relative difference between Schwinger's equation and direct calculation is on the order of 10^{-5} which is negligible compared to our measurement uncertainty.

To measure the flux of synchrotron radiation as a function of the angle ψ, a filter radiometer with an active area A at a distance of r from the tangent point is scanned in the vertical direction (perpendicular to the orbital plane) as shown in Fig. 2. The irradiance responsivity of the filter radiometer $R(\lambda)$ is defined as the ratio of the signal (in A) to the irradiance (in $\mathrm{W/cm^2}$) of a uniform field of incident radiation in the area A at wavelength λ. $R(\lambda)$ can be determined experimentally by using a uniform and tunable monochromatic source.

For the measurement of the angular distribution of synchrotron radiation, the signal of the filter radiometer from exposure to synchrotron radiation at an angle of ψ is

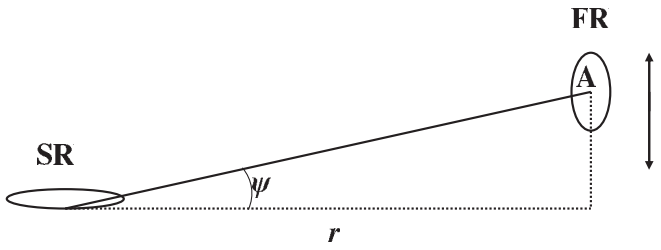

FIG. 2. Geometry for measuring the angular distribution of synchrotron radiation using a filter radiometer with an active area of A. r is the distance from the tangent point to the filter radiometer and ψ is the off-orbital-plane angle extended by a fixed point in the active area of the filter radiometer to the tangent point.

$$S(\psi) = \int E(\psi, \lambda) R(\lambda) d\lambda, \tag{4}$$

where the mean spectral irradiance, $E(\psi, \lambda)$, is defined as

$$E(\psi, \lambda) = \frac{\Phi(\psi, \lambda)}{A}$$

with $\Phi(\psi, \lambda)$ the total spectral flux of synchrotron radiation (in W/cm) incident on the active area of the filter radiometer. In Eq. (4), we assume that the filter radiometer has a uniform response across the active area A.

If the mean spectral irradiance $E(\psi, \lambda)$ is a smooth function of the wavelength, then we can expand $E(\psi, \lambda)$ about a fixed wavelength λ_0 as

$$E(\psi, \lambda) = E(\psi, \lambda_0) + E^{(1)}(\psi, \lambda_0)(\lambda - \lambda_0) + \frac{E^{(2)}(\psi, \lambda_0)}{2}(\lambda - \lambda_0)^2 + \cdots, \tag{5}$$

where $E^{(1)}$ and $E^{(2)}$ are the first and second derivatives of E with respect to λ. Combining Eqs. (4) and (5), we have

$$S(\psi) = E(\psi, \lambda_0) \int R(\lambda) d\lambda + E^{(1)}(\psi, \lambda_0) \times \int (\lambda - \lambda_0) R(\lambda) d\lambda + \frac{E^{(2)}(\psi, \lambda_0)}{2} \times \int (\lambda - \lambda_0)^2 R(\lambda) d\lambda + \cdots. \tag{6}$$

If we choose λ_0 to be the response-weighted mean wavelength of the filter radiometer as defined by

$$\lambda_0 = \frac{\int \lambda R(\lambda) d\lambda}{\int R(\lambda) d\lambda}, \tag{7}$$

then the second term on the right-hand side of Eq. (6) vanishes and Eq. (6) becomes

$$S(\psi) = E(\psi, \lambda_0) \int R(\lambda) d\lambda + \frac{E^{(2)}(\psi, \lambda_0)}{2} \times \int (\lambda - \lambda_0)^2 R(\lambda) d\lambda + \cdots.$$

Because the wavelengths of the filter radiometers used in this work (in the hundreds of nm) are much longer than the critical wavelengths of the electron energies used at SURF III (8.5 nm at 380 MeV, for example), the synchrotron radiation flux decreases very slowly as a function of the wavelength at these filter radiometer wavelengths and the second derivative of the synchrotron radiation radiant flux with respect to wavelength is rather small. This, and the fact that filter radiometers used in this work have a narrow bandwidth of about 10 nm, makes the second and higher order terms in the above equation negligible. Numerical calculations confirm that the typical contribution from the second order term to the total observed signal in this work is less than 1×10^{-3}, below our measurement uncertainty of several tenths of a percent. Thus, we can approximate the above expression with

$$S(\psi) = E(\psi, \lambda_0) \int R(\lambda) d\lambda \tag{8}$$

and in turn

$$E(\psi, \lambda_0) = \frac{S(\psi)}{R_i}, \tag{9}$$

where the integrated irradiance responsivity, R_i, is defined as

$$R_i = \int R(\lambda) d\lambda. \tag{10}$$

Equation (9) states that one can derive the average spectral irradiance of synchrotron radiation over the active area of a filter radiometer by using the measured signal of the filter radiometer as a function of the angle and the integrated irradiance responsivity of the filter radiometer at the response-weighted mean wavelength of the filter radiometer. The result can then be compared with theoretical calculation by substituting Schwinger's equation of Eq. (3) into

$$E(\psi, \lambda_0) = \frac{n_e \int_A \left(\frac{d^2 I(\lambda_0)}{d\lambda d\Omega}\right) \frac{1}{r^2} ds}{A}, \tag{11}$$

where n_e is the total number of electrons orbiting in the storage ring and the surface integral is over the area A of the active area of the filter radiometer.

III. EXPERIMENTAL SETUP

Measurements were performed on a white-light beamline [20,21] at SURF III as shown in Fig. 3. The beamline was designed so that the detector package mounted in the end-user's chamber, located some 6 m away from the tangent point, can be exposed to synchrotron radiation without any obstruction, such as windows, in the path of the radiation. All the limiting apertures along the beamline have a diameter large enough to allow synchrotron radiation emitted at ± 10 mrad above and below the orbital plane to reach the end chamber. This wide opening also reduces the effect of diffraction that could be significant at longer wavelengths. To minimize scattering of light from the stainless vacuum wall of the beamline, a series of carbon-film coated baffles were installed throughout the beamline. All baffles are in a cone shape and act as light traps.

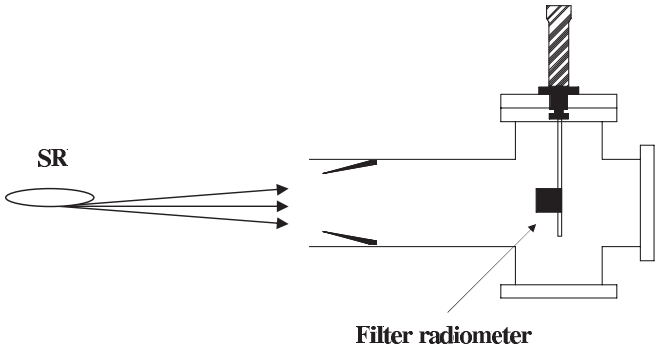

FIG. 3. Schematic diagram of the end chamber for measuring angular distribution of synchrotron radiation.

Inside the end chamber, a filter radiometer used for this measurement can be mounted on a linear stage for vertical movements. The stage is controlled by a stepping motor which controls the movement via a linear vacuum feedthrough. Photocurrent from the filter radiometer is measured by a digital ammeter. A computer that controls the linear stage records the photocurrent from the ammeter. All the storage ring parameters are also recorded by the computer in real time from the SURF III control center through an Ethernet connection. These parameters include: electron energy, electron beam current, orbital radius, and beam size and position information. All photocurrent data are normalized by the electron beam current to compensate for the gradual decay of beam current during the time of the angular distribution measurement. A discussion of the construction and calibration of the filter radiometers is given in the next section.

A detailed discussion of the measurements of the fundamental parameters of the storage ring of SURF III was given elsewhere [18]. Here, we give a brief overview of three parameters that we used for numerical calculation of the Schwinger's equation, namely, electron energy, orbital radius, and electron beam current.

The electron energy and orbital radius are derived from the measured magnetic flux density on orbit and the frequency of the driving radio-frequency (rf) field by the synchronicity condition and Lorentz-force equation [22]. At SURF III, the magnetic field is monitored by several field probes [18] with a relative measurement uncertainty of 10^{-4} and the frequency of the rf field is synchronized with a rubidium atomic clock which has a relative uncertainty of 10^{-10}. This corresponds to an uncertainty of 10^{-4} for the electron energy and 10^{-10} for the orbital radius. Calculation using Schwinger's equation shows that the

combined uncertainty of radiant flux at the wavelengths of interest from these uncertainties is on the order of 10^{-5}, well below the uncertainty we achieved in this measurement. The relative insensitivity of the radiant flux calculation to the measurement uncertainties of electron energy and orbital radius is because the wavelengths discussed here are much longer than the critical wavelengths of the operating electron energies.

The electron beam current at SURF III is measured optically by using a silicon photodiode to monitor the emitted synchrotron radiation flux [23]. The scale of the absolute current is determined by an electron-counting method where the synchrotron radiation flux from each electron in the storage ring can be measured when the total number of electrons in the storage ring is less than a few thousand. At SURF III, electron counting is performed regularly at various energies to counter any drift from electrical and optical systems. The estimated uncertainty in the electron beam current is 2×10^{-3}. Because the radiant flux of synchrotron radiation is proportional to the electron beam current, the uncertainty of electron beam current translates directly to the radiant flux uncertainty. Presently, this is the dominant uncertainty at SURF III as compared with the uncertainties caused by electron energy and orbital radius measurements.

One more parameter that is required for the calculation of the radiant flux of synchrotron radiation irradiating the detector using Eq. (11) is the distance, r, of the detector front surface to the tangent point. We measured r using two techniques; optical triangulation and direct measurement using a laser range finder. In optical triangulation, a filter radiometer consisting of a silicon photodiode, a 334 nm filter, and a 500 μm pin hole, was mounted on the translation stage in the end chamber. At about 1.5 m from the tangent point, another aperture of about 1 mm in size was mounted on a second linear stage. To measure r, the 1 mm aperture was positioned at different vertical positions by its linear stage and each of their corresponding beam centers at the end chamber was located by the 334 nm filter radiometer. The distance r can be derived by simple geometric consideration using the aperture displacement and the corresponding beam center displacement in the end chamber in conjunction with the distance between the aperture and the filter radiometer which was measured by a laser range finder.

To verify the result from the optical triangulation method, an independent direct measurement technique was used. We made use of a fiducial ring as our distance reference. This fiducial ring was carved around the storage ring during the construction of SURF III and was designed to be concentric to the electron orbit and with known radius. We measured the shortest distance from the front surface of the detector to the fiducial ring using a laser range finder. This measured distance, along with the known radius of the fiducial ring and the radius of the electron orbit, can be used to derive the distance r. By using both techniques, we found the distance from the tangent point to the front of the detector to be 610.0 cm by the optical triangulation technique and 609.8 cm by direct measurement using the laser range finder. The difference is less than 0.03%, consistent with the estimated uncertainty of our measurements.

Finally, one has to consider the effect of the vertical size of the electron beam in the storage ring. At SURF III, the smallest vertical size of the electron beam is typically about 30 μm (in full-width-half-max) [24]. Calculation shows that such a small size has a negligible difference as compared to that of a point source for our measurements in this work [25].

IV. CONFIGURATION AND CALIBRATION OF FILTER RADIOMETERS

Filter radiometers based on narrow-band interference filters were constructed at NIST and used to measure the radiant flux of synchrotron radiation. While the spectral resolution of filter radiometers is lower than a typical monochromator-detector system, filter radiometers are superior in terms of their high sensitivity, low polarization dependence for normal incident radiation, compact size, vacuum compatibility, and high stability. In addition, filter radiometers are routinely calibrated at NIST with high accuracy.

Shown in Fig. 4 is a schematic of the three filter radiometers used for this work. Each filter radiometer has a circular precision aperture of 3.5 mm in diameter, a roughened quartz plate, an interference filter, and a silicon photodiode. The roughened quartz plate is used as a diffuser to avoid interference effects when the filter radiometer is calibrated with laser light (see below). Three

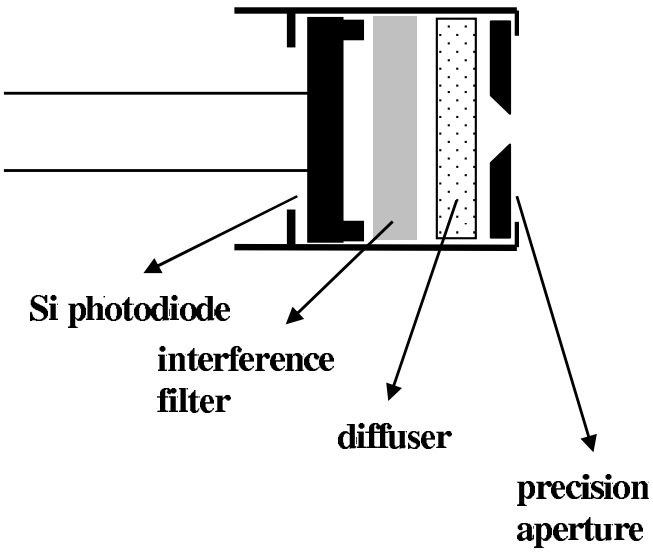

FIG. 4. Schematic diagram of a filter radiometer for synchrotron radiation characterization.

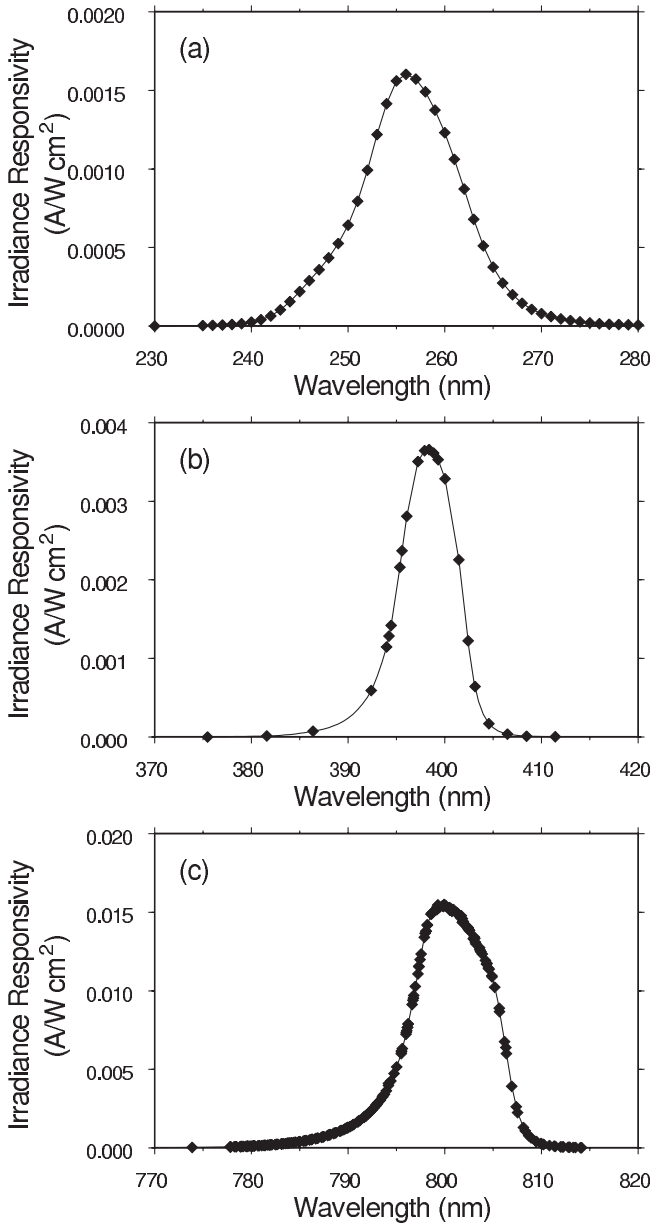

FIG. 5. Measured irradiance responsivities of filter radiometers with (a) FR1, (b) FR2, and (c) FR3.

commercial filters with approximate center wavelengths of 254, 400, and 800 nm were used for the three filter radiometers, FR1, FR2, and FR3, respectively. All three filters have a bandwidth on the order of 10 nm.

Calibration of the spectral irradiance responsivity of the filter radiometers was performed at two facilities at NIST; a cryogenic-radiometer based radiometric beamline [26,27] at SURF III for FR1, and the spectral irradiance and radiance responsivity calibrations using uniform sources [28] (SIRCUS) facility for FR2 and FR3. The radiometric beamline at SURF III is mainly designed for calibration of spectral power responsivity in the UV and VUV range using a monochromatized synchrotron radiation beam. To measure a detector's irradiance responsivity, a technique [29] of raster scanning the active area of a detector with the probing beam can be used. Shown in Fig. 5(a) is the measured irradiance responsivity for the FR1 using this technique with an estimated uncertainty of 0.5%.

TABLE I. Filter radiometer parameters for FR1, FR2, and FR3 as derived from irradiance calibration. λ_0 is the response-weighted mean wavelength and R_i is the integrated irradiance responsivity (see text).

	FR1	FR2	FR3
λ_0 in nm	256.5	397.8	799.8
R_i in A/(W/cm^2) nm	0.020 77	0.027 59	0.1630

The second calibration facility, SIRCUS, makes use of a tunable laser system to calibrate detectors with a primary scale also derived from a cryogenic radiometer. For irradiance responsivity measurement, an integrating sphere is used to transform the laser beam into a uniform Lambertian source before the beam irradiates the device under test. The irradiance responsivity of the device under test is derived by comparing the signal from the device to that of a transfer standard trap detector which includes a calibrated aperture at the radiation entrance to convert this trap detector into a high-accuracy irradiance meter. The trap detector has been calibrated for spectral power responsivity against a cryogenic radiometer. The measured irradiance responsivities of FR2 and FR3 are shown in Figs. 5(b) and 5(c) with an estimated uncertainty of 0.1%.

As discussed previously in Eqs. (7) and (10), the only required quantities from a filter radiometer for angular distribution measurement of synchrotron radiation are the response-weighted mean wavelength, λ_0, and the integrated irradiance responsivity, R_i. The results of these two parameters for all three filter radiometers calculated from their irradiance response calibrations using numerical integration are summarized in Table I.

V. RESULTS AND DISCUSSION

Shown in Fig. 6 is the measured photocurrent from FR1 as a function of the vertical displacement when exposed to synchrotron radiation emitted by a 285 MeV electron beam. The signal has been normalized to 1 mA of SURF electron beam current using the SURF actual current collected real-time during the course of the measurement. Figure 6 clearly shows the characteristics of the double-peak structure predicted by Schwinger's equation. To convert the vertical displacement into angle, we make use of the measured 610.0 cm distance from the filter radiometer to the tangent point discussed in Sec. III and a center on-orbit position of the filter radiometer which is obtained by fitting the center minimum region with a quadratic polynomial. An example of finding the center on-orbit position by fitting with a polynomial is shown in Fig. 7. The center

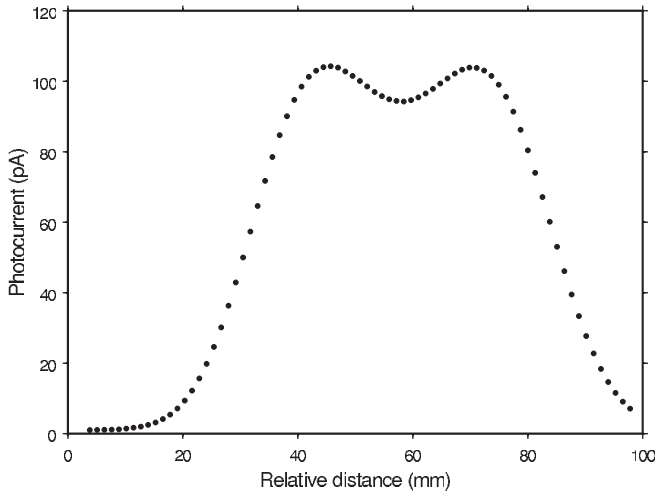

FIG. 6. Photocurrent measured as a function of the vertical displacement from FR1 with 285 MeV electron energy. The signal is normalized to 1 mA of SURF current.

position can be easily derived from the fitted parameters with an accuracy of about 25 μm.

The mean spectral irradiance of the synchrotron radiation inside the aperture of the filter radiometer can be determined from Eq. (9) using the parameters of the filter radiometer listed in Table I and the measured photocurrent such as the measurement shown in Fig. 6. The measured spectral irradiance can then be compared to the calculation from Schwinger's equation using Eq. (11). Figure 8 demonstrates the comparison between the calculated and the measured spectral irradiance of synchrotron radiation at 256.5 nm using FR1 with SURF energies of 380, 285, 180 MeV. We also include results from 105 MeV for comparison [30]. As the SURF energy decreases, the irradiance at 256.5 nm also decreases and the angular distribution changes from a two-peak structure to a single peak structure with good agreement with the calculated values. Furthermore, Fig. 9 shows the angular distribution at wavelengths of 256.5, 397.8, and 799.8 nm measured with all three filter radiometers for a fixed SURF energy of 380 MeV compared with calculation. The angular distribution broadens with increasing wavelength coupled with a deceasing irradiance near the center.

The agreements between the measured spectral irradiance and theory are found to be within 0.5% in the region

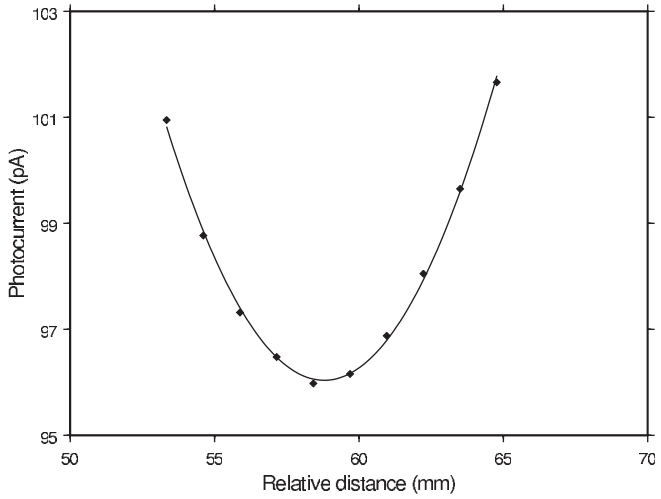

FIG. 7. Measured photocurrent as a function of vertical displacement in the center minimum region by FR1 with 380 MeV SURF current. The line is the best fit curve to a quadratic polynomial for the determination of the on-orbit position.

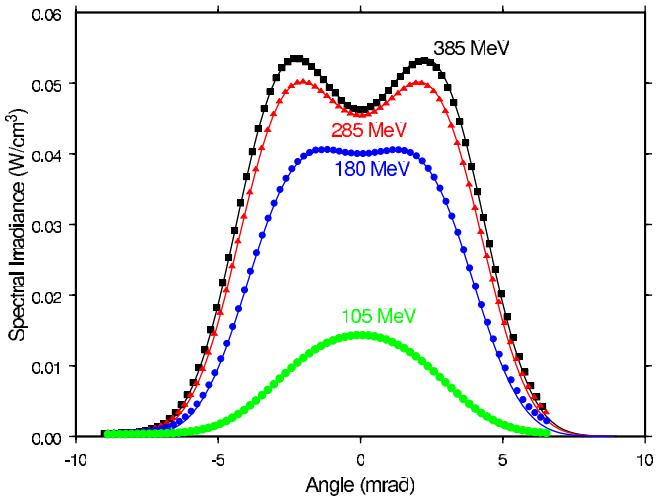

FIG. 8. (Color) Absolute irradiance measurement of the angular distribution of synchrotron radiation at 256.5 nm using FR1. All results are normalized to 1 mA of SURF III current with the top curve measured at a SURF energy of 380 MeV followed by 285, 180, and 105 MeV. The lines are the results of calculations using Schwinger's equation.

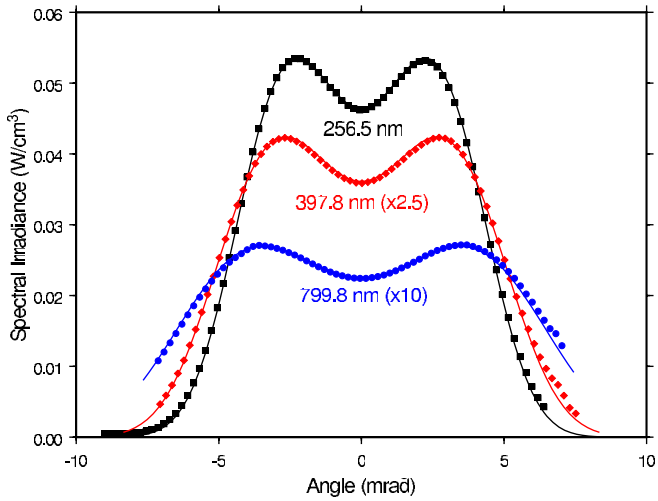

FIG. 9. (Color) Absolute irradiance measurement of the angular distribution of synchrotron radiation at a SURF energy of 380 MeV. All results are normalized to 1 mA of SURF III current with the top curve measured at 256.5 nm using FR1 followed by 397.8 nm using FR2, and 799.8 nm using FR3. The lines are the results of calculations using Schwinger's equation.

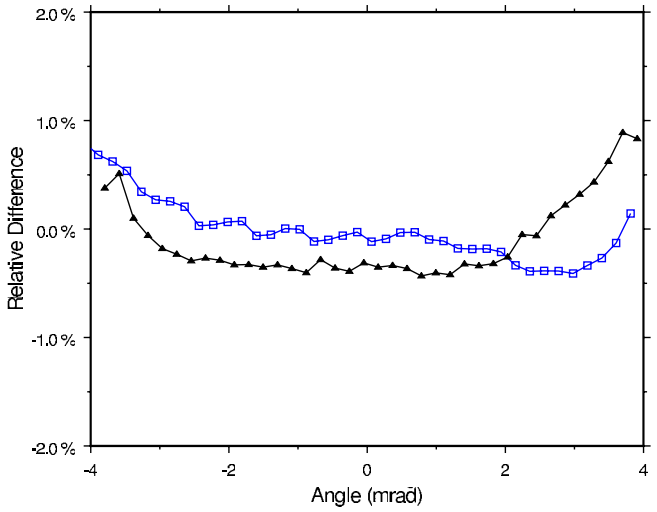

FIG. 10. (Color) Relative difference between measurement and theory in percent, open squares: 285 MeV SURF energy at 256.5 nm; and, filled triangles: 380 MeV SURF energy at 799.8 nm.

TABLE II. Components of the combined relative standard uncertainty for absolute flux measurements.

Source of uncertainty	Estimated uncertainty (%)
Electron energy	0.1
Beam current	0.2
Orbital radius	10^{-8}
Filter radiometer calibration	0.5
Stray light	0.2
Combined	0.6

from −4 to 4 mrad for the results shown in Figs. 8 and 9. Figure 10 demonstrates two examples of the relative difference between measurement and theory. The difference is within the combined relative standard uncertainty estimated at 0.6% for this work as listed in Table II. For large measurement angles, the measured irradiance is generally larger than the calculated value indicating a possible contribution from scattered light. We are currently working to further reduce such scattering. Finally, we note that during the course of this work, great care was given to avoid radiation damage on the filter radiometers. In addition to the low SURF energy of less than 380 MeV, we limited the amount of exposure time for each filter radiometer to synchrotron radiation and the SURF current during exposure to less than 100 mA. Each measurement was repeated several times and we found no signs of degradation on all three filter radiometers.

VI. CONCLUSION

We have measured and confirmed the Schwinger theory on the absolute radiant flux and the angular distribution of synchrotron radiation at wavelengths from near IR to UV at various electron energies. The agreement between measurement and theory is better than 0.5% for a wide range of angles. In practice, such agreement also demonstrates the accuracy of SURF III and reinforces the notion of SURF III as an absolute calculable source. Practical applications include using radiation from SURF III to calibrate conventional light sources. This is particularly important for UV to x-ray sources, such as a deuterium lamp, where calibration uncertainty can be much reduced by comparing with synchrotron radiation. Such calibration has already being successfully conducted at NIST against radiation from SURF III.

ACKNOWLEDGMENTS

The authors appreciate the continued support from SURF staff of Alex Farell, Mitch Furst, and Edward Hagley. We would also like to thank Thomas Lucatorto for helpful discussions.

[1] J. Schwinger, Phys. Rev. **75**, 1912 (1949).
[2] See, for example, *Synchrotron Radiation Sources—A Primer*, edited by Herman Winick (World Scientific, Singapore, 1995); Philip John Duke, *Synchrotron Radiation—Production and Properties* (Oxford, New York, 2000).
[3] F. R. Elder, R. V. Langmuir, and H. C. Pollock, Phys. Rev. **74**, 52 (1948).
[4] D. H. Tomboulian and P. L. Hartman, Phys. Rev. **102**, 1423 (1956).
[5] K. Codling and R. P. Madden, J. Appl. Phys. **36**, 380 (1965).
[6] G. Bathow, E. Freytag, and R. Haensel, J. Appl. Phys. **37**, 3449 (1966).
[7] D. Lemke and D. Labs, Appl. Opt. **6**, 1043 (1967).
[8] E. Pitz, Appl. Opt. **8**, 255 (1969).
[9] P. J. Key, Metrologia **6**, 97 (1970).
[10] D. L. Ederer, E. B. Soloman, S. C. Ebner, and R. P. Madden, J. Res. Natl. Bur. Stand. Sect. A **79**, 761 (1975).
[11] P. J. Key and R. C. Preston, Appl. Opt. **16**, 2477 (1977).
[12] A. R. Schaefer, R. D. Saunders, and L. R. Hughey, Opt. Eng. **25**, 892 (1986).
[13] M. Stock, J. Fischer, R. Friedrich, H. J. Jung, R. Thornagel, G. Ulm, and B. Wende, Metrologia **30**, 439 (1993).
[14] T. Masuoka, K. Kitamura, T. Oshio, M. Nishi, H. Onuki, A. Ejiri, Y. Morioka, and M. Nakamura, Nucl. Instrum. Methods **152**, 219 (1978).
[15] Y. Tang and F. Li, Nucl. Instrum. Methods Phys. Res., Sect. A **337**, 598 (1994).
[16] F. Riehle and B. Wende, Opt. Lett. **10**, 365 (1985).
[17] N. P. Fox, P. J. Key, F. Riehle, and B. Wende, Appl. Opt. **25**, 2409 (1986).
[18] U. Arp, R. Friedman, M. L. Furst, S. Makar, and P. S. Shaw, Metrologia **37**, 357 (2000).

[19] J. D. Jackson, in *Classical Electrodynamics* (Wiley, New York, 1975), 2nd ed., Chap. 14.
[20] P. S. Shaw, D. Shear, R. J. Stamilio, U. Arp, H. W. Yoon, R. D. Saunders, A. C. Parr, and K. R. Lykke, Rev. Sci. Instrum. **73**, 1576 (2002).
[21] P. S. Shaw, U. Arp, H. W. Yoon, R. D. Saunders, A. C. Parr, and K. R. Lykke, Metrologia **40**, S124 (2003).
[22] H. Wiedemann, *Particle Accelerator Physics* (Springer-Verlag, New York, 1993).
[23] A. R. Schaefer, L. R. Hughey, and J. B. Fowler, Metrologia **19**, 131 (1984).
[24] U. Arp, Nucl. Instrum. Methods Phys. Res., Sect. A **462**, 568 (2001).
[25] U. Arp, J. Res. Natl. Inst. Stand. Technol. **107**, 419 (2002).
[26] P. S. Shaw, K. R. Lykke, R. Gupta, T. R. O'Brian, U. Arp, H. H. White, T. B. Lucatorto, J. L. Dehmer, and A. C. Parr, Appl. Opt. **38**, 18 (1999).
[27] P. S. Shaw, T. C. Larason, R. Gupta, S. W. Brown, R. E. Vest, and K. R. Lykke, Rev. Sci. Instrum. **72**, 2242 (2001).
[28] S. W. Brown, G. P. Eppeldauer, and K. R. Lykke, Metrologia **37**, 579 (2000).
[29] P. S. Shaw, R. Gupta, and K. R. Lykke, Appl. Opt. **41**, 7173 (2002).
[30] One should note that low SURF energies, such as 105 MeV, are outside the standard energy range where electron current was calibrated based on electron counting and one expects large uncertainty in the electron current measured by a monitoring detector at SURF III. As a consequence of our angular distribution measurement at 105 MeV, we have determined that the measured electron current is off by 6% at 105 MeV. The calculated values shown in Fig. 8 for 105 MeV reflect this correction.